Thermodynamic constraints on the diversity of microbial ecosystems

Jacob Cook[1,2], Samraat Pawar[3‡*], Robert G. Endres[1,2‡*]

1 Department of Life Sciences, Imperial College, London SW7 2AZ, United Kingdom
2 Centre for Integrative Systems Biology and Bioinformatics, Imperial College, London SW7 2AZ, United Kingdom
3 Department of Life Sciences, Imperial College London, Silwood Park Campus, Ascot SL5 7PY, United Kingdom

‡These authors contributed equally to this work.
* s.pawar@imperial.ac.uk, r.endres@imperial.ac.uk

Abstract

Most biological processes are driven by non-equilibrium thermodynamics, but despite significant progress in theoretical ecology the constraints this places on ecosystem dynamics has been barely considered. Microbial ecosystems represent a natural place to begin this consideration, as many of the ways they interact, such as metabolite production and cross-feeding, can be described in thermodynamic terms. Previous work considered the impact of thermodynamics such as the rate-yield trade-off on individual species' competitive ability, but restrained from analyzing complex dynamical systems. To address this gap we developed a thermodynamic microbial consumer-resource model with fully reversible reaction kinetics, which allows direct consideration of free-energy dissipation. Using this model, we show that ecosystem diversity increases with supplied free energy, because greater availability of free energy allows for faster ecosystem development. Thus, when species from the initial community begin to go extinct more possible niches have been formed, facilitating increased diversity. Our model also shows that the inclusion of species utilising near-to-equilibrium reactions increases diversity under conditions of low free-energy supply. At low free energy supply thermodynamic interaction types reach comparable strength to the conventional (competition and facilitation) interactions yielding a more nuanced classification of interactions, and emphasising the key role thermodynamics plays in the dynamics. Though our model is valid for all microbial ecosystems where diversification from an initial substrate occurs it is of particular use when the initial substrate is recalcitrant (low-free energy).

Author summary

There is a growing interest in microbial ecosystems due to their important role in carbon cycling and human health. Although our understanding of thermodynamic constraints on individual cells is rapidly improving, the impact of these constraints on complex microbial ecosystems remains largely unexplored theoretically and empirically. To address this we develop a novel microbial consumer-resource model which allows thermodynamic efficiency and entropy production to be calculated directly. We show that greater free energy availability allows for a faster rate of niche generation, leading to higher final species diversities. We also show that when the free energy availability is low, species with reactions close to thermodynamic equilibrium are selected for leading

to more diverse high efficiency communities. When we compare the strength of different interaction types we find that though the conventional interaction types (competition and facilitation) are generally the strongest, thermodynamic interaction types are significant. Taken together our results suggest that non-equilibrium thermodynamics cannot be neglected when describing the dynamics of microbial ecosystems.

Introduction

The application of non-equilibrium thermodynamics has met with significant success across quantitative biology granting particularly strong insights into kinetic proofreading [1] and sensing accuracy [2]. Additionally, equilibrium thermodynamic models have been frequently used in ecology to predict species abundance distributions [3]. Despite all this the fundamental constraints that thermodynamics places on microbes are rarely considered in microbial ecosystem models. When thermodynamic constraints are mentioned statements are often very generalising e.g. that energy cannot be spontaneously created or that enzyme rate constants are subject to some form of constraint. Beyond these fairly obvious observations there are two more complex thermodynamic mechanisms likely to effect microbes. These are the thermodynamic inhibition reactions experienced close to thermodynamic equilibrium, and the fact that metabolic networks can only incorporate thermodynamically feasible reactions (so there is a net free-energy dissipation). Both of these can act to constrain microbial growth, and thus impact ecosystem dynamics, but are little discussed. Models of the impact of thermodynamic inhibition on microbial ecosystems have been developed in the anaerobic digestion literature [4]. This has been recently extended to study whether thermodynamics leads to distinct ecological strategies [5] and to explain the coexistence of multiple species on a single substrate [6]. However, in both these cases only a small number of interacting species is considered rather than a large number of species that would be expected in the real microbial ecosystems.

Another fundamental constraint often not considered in microbial ecology is the one of cells finite proteome. Due to the finite small cells size a higher expression of a given type of protein must always come at the expense of lowered expression of other types of proteins. Attempts to capture this constraint is often done by introducing a fixed "enzyme budget" which has to be divided between nutrients [7]. However, the inclusion of a comprehensive and rigorous proteome allocation constraint has not been done, despite the fact that this constraint of a finite proteome is known to impact microbial growth [8, 9]. Given that mechanistic models of this constraint have already been developed [10] in a single population, it should be readily incorporatable into microbial ecosystem models. This mechanistic physics-motivated model with fluxes and conservation laws was capable of explaining several empirically observed growth laws. So, extending this model to microbial ecosystems offers real potential to for insight into their dynamics.

There is substantial debate in the literature about the relative importance of competitive and cooperative interactions to microbial ecosystems. Some of this work has taken a phenomenological approach to empirically determine whether interactions between species are negative (competitive) or positive (cooperative) [11]. Reconstruction of full metabolic models can allow for a more mechanistic understanding of these interactions, by considering substrate overlap (competition) and metabolite production (facilitation) [12]. Though metabolic models of this type both provide a very detailed view of ecosystems and take thermodynamic effects properly into account, their huge complexity means they are computationally unfeasible to simulate for real world ecological processes such as ecosystem assembly. We thus take the middle road in terms of model complexity by incorporating non-equilibrium thermodynamics into a

conventional consumer-resource model with cross feeding [13, 14]. Doing this introduces a dependence of reaction rate on product concentration, potentially leading to the emergence of novel interaction types between species via products rather than via substrates. Previous work has not considered either of these novel interaction types or the impact of thermodynamics on ecosystem dynamics in general. This represents a significant limitation on our ability to understand the emergent effects of the intrinsic trade-offs and limitations experienced by species upon broader ecosystem properties such as diversity.

Here we developed a model that explicitly incorporates both thermodynamic and proteome constraints. We then utilise this model to ask what the emergent impact on ecosystem diversity from fundamental thermodynamics constraints is. We found that increased substrate free energy significantly increases final species diversity, as greater free energy availability allows faster ecosystem development, and hence faster niche development as the substrate diversifies. We also found that only when substrate free energy is low does allowing near-equilibrium reactions increase the final diversity. This is because only here is the significant additional free energy captured through using near-equilibrium reactions. Finally, we found that the strength of thermodynamic interactions could be of comparable strength to the conventional interaction types (competition and facilitation), highlighting the impact of thermodynamics on the ecosystem dynamics. Taken together our results show the importance of considering thermodynamic effects when modelling microbial ecosystems. Understanding these effects is vital for understanding ecosystems with low free energy availability such as anaerobic ecosystems or systems diversifying from recalcitrant substrates. These types of microbial ecosystems are common but less studied, and understanding of their dynamics is vital to understanding the impact of microbes on wider ecosystems and the climate.

Model

The thermodynamic microbial consumer-resource model that we developed is shown in Fig 1A. Here, a single resource is supplied with rate κ, and consumed by the various microbial species producing metabolic byproducts, which can also be consumed. All metabolites, whether supplied or not, are then diluted out of the system by dilution factor ρ. These resource dynamics can be stated as

$$\frac{dC_\alpha}{dt} = \kappa\delta_{\alpha,1} - \rho C_\alpha + \sum_{i=1}^{B} \left(p_{i,\alpha}(\mathbf{C}) - c_{i,\alpha}(\mathbf{C})\right) N_i, \tag{1}$$

where C_α is the concentration of metabolite α, $\delta_{\alpha,\beta}$ is the Kronecker delta, B is the number of species in the ecosystem, N_i is the population of species i, $p_{i,\alpha}$ is the (per cell) rate that species i produces metabolite α, and $c_{i,\alpha}$ is the (per cell) rate that species i consumes metabolite α.

Proteome trade-offs

In order to determine species growth rates we developed a minimal cell model (shown in the magnification in Fig 1A). This model comprises of four key processes: (1) The cell exchanges metabolites with its environment. For the sake of simplicity we assume that the intracellular metabolite concentrations are equal to the environmental concentrations. This simplifying assumption is appropriate to study cellular thermodynamics as processes which maintain differences between intracellular and environmental necessarily consume free energy, and so the same limits on efficiency will hold. (2) Within the cell metabolites are broken down into lower free-energy

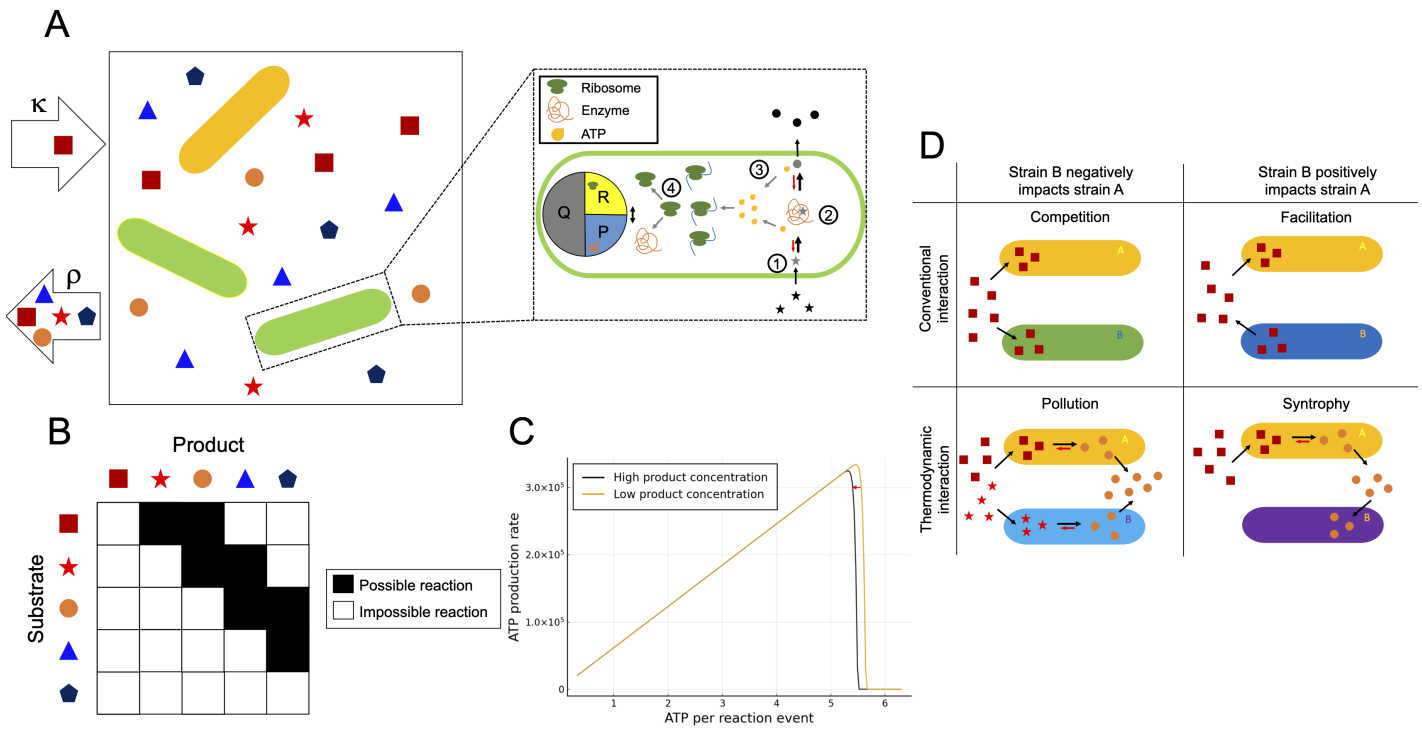

Fig 1. Overview of thermodynamic microbial consumer-resource model. (a) A singular resource is supplied with rate κ, and is diversified into a broader range of metabolites by the microbes. All metabolites are diluted out of the system with constant dilution factor ρ. (magnification) Schematic of our cellular model, comprising four key processes: (1) the take up of metabolites by the cell, (2) the break down of these metabolites into waste products (Eqs 12–13), (3) the generation of ATP through this process (Eq 8), and (4) the use of this ATP to drive protein synthesis (Eqs 2–3). The microbial cells proteome is partitioned into three compartments: A constant housekeeping protein compartment (Q), a ribosome compartment (R), and a metabolic protein compartment (P). The size of the ribosome compartment can be increased at the expense metabolic protein compartment, and vice versa. When metabolite conditions are constant the growth rate is solely determined by the outcome of this trade-off. (b) An example matrix of possible metabolic reactions. Metabolites can only react to form new metabolites that are one or two positions lower on the metabolite free-energy hierarchy. (c) Plot of the type of thermodynamic trade-off that emerges from our model. Our trade-off shows a linear increase of ATP production rate with an increase in ATP per reaction event (η), up to the point where thermodynamic inhibition becomes significant. The position of optimal η value shifts as environmental metabolite concentrations change. (d) Schematic showing the four possible cell-cell interaction types in our model. Competition and facilitation interactions emerge in all consumer-resource models that allow for the production of resources. In addition to these, there are two thermodynamic interaction types: "pollution" where one species produces a metabolite that causes thermodynamic inhibition to the other species, and "syntrophy" where a species consumes a metabolite that is thermodynamically inhibiting the other species.

metabolites. This process is thermodynamically reversible in contrast to the conventionally used Michaelis–Menten kinetics (for a discussion of different enzyme kinetic schemes see S1 Appendix). (3) This breakdown of metabolites into lower free-energy metabolites allows free-energy to be transduced via the production of ATP. (4) This ATP is subsequently used to fuel protein synthesis [8–10]. It is assumed that the proteome of each cell can be partitioned into three compartments: a ribosome compartment R, a metabolic protein compartment P, and a compartment for all other proteins required by the cell Q (termed "housekeeping"). As the housekeeping compartment is assumed to be constant a direct trade-off between the fraction of the

proteome dedicated to ribosomes and the fraction dedicated to metabolic proteins arises.

In our model the growth rate of any given microbial species is determined by the total rate at which ribosomes synthesize proteins (process 4 in Fig 1A). This can be modelled by assigning each species (i) two internal variables, the internal energy (ATP) concentration a_i and the ribosome fraction $\phi_{R,i}$. The cellular growth rate depends on both quantities and can be expressed as

$$\lambda_i(a_i, \phi_{R,i}) = \frac{\gamma(a_i) f_b \phi_{R,i}}{n_R}, \tag{2}$$

where $\gamma(a_i)$ is the effective translation elongation rate, f_b is the average fraction of ribosomes bound and translating, and n_R is the number of amino acid per ribosome. As we assume that protein synthesis is an irreversible process the effective translation elongation rate is taken to obey Michaelis–Menten kinetics with respect to the energy concentration

$$\gamma(a_i) = \frac{\gamma_m a_i}{K_\gamma + a_i}, \tag{3}$$

where γ_m is the maximum elongation rate, and K_γ is a half saturation constant. Using this growth rate in Eq 2 the population dynamics can then be specified as

$$\frac{dN_i}{dt} = (\lambda_i(a_i, \phi_{R,i}) - d_i) N_i, \tag{4}$$

where d_i is the rate of biomass loss. We now want to consider the dynamics of the internal variables, starting with the ribosome fraction dynamics which can be described by

$$\frac{d\phi_{R,i}}{dt} = \frac{1}{\tau_g} \left(\phi_R^*(a_i) - \phi_{R,i} \right), \tag{5}$$

where $\tau_g = \log_2(100)/\lambda_i$ (see S1 Appendix) is the characteristic time scale for growth and $\phi_R^*(a_i)$ is the ribosome fraction that the cell aims to reach when it has a specific energy concentration a_i. This is termed the ideal ribosome fraction and following Eq 3 is assumed to have the following energy dependence with saturation

$$\phi_R^* = \frac{a_i}{K_\Omega + a_i}(1 - \phi_Q), \tag{6}$$

where K_Ω is a half saturation constant and ϕ_Q is the housekeeping protein fraction. The other internal variable considered in our model is the energy concentration which has dynamics described by

$$\frac{da_i}{dt} = J_i - \chi m \lambda_i - a_i \lambda_i, \tag{7}$$

where J_i is the ATP production rate for species i, χ is ATP use per elongation step, and m is the total mass of the cell (in units of amino acids). The second term in Eq 7 corresponds to the energy use due to protein translation and the third term corresponds to the dilution of energy due to cell growth. A complete derivation of our proteome model can be found in S1 Appendix.

ATP production

To determine each species' internal energy dynamics the rate at which ATP is produced (process 3 in Fig 1A) must be determined. To obtain this rate we consider thermodynamic aspects. Fig 1B shows the general pattern of possible reactions in our model for an example case with a small number of metabolites ($M = 5$). We immediately notice that due to the explicit thermodynamically reversibility of our

model only reactions descending in free energy are permitted. Further to this we assume that every step down the metabolite hierarchy represents a meaningful change in biochemistry. A reaction that takes a substantial number of steps down this hierarchy would therefore require a large and complex protein machinery to accomplish all the required changes. To better capture this complexity we choose to model this situation as the species possessing multiple reactions (in a chain) rather than a single very complex reaction. Hence, in our model no direct links between metabolites separated by more than two positions on the metabolite hierarchy are allowed. Each species (i) is assigned a random subset (O_i) of this set of possible reactions. The ATP production rate can then be found as

$$J_i = \sum_{\alpha \in O_i} \eta_{\alpha,i} q_{\alpha,i}(E_{\alpha,i}, S_\alpha, W_\alpha), \tag{8}$$

where $\eta_{\alpha,i}$ is the number of ATP generated by species i per reaction event of reaction α, $q_{\alpha,i}$ is species i's (mass specific) reaction rate for reaction α, $E_{\alpha,i}$ is the copy number of enzymes for reaction α that species i possesses, S_α is the concentration of reaction α's substrate, and W_α is the concentration of of reaction α's waste product. The enzyme copy number depends on metabolic protein fraction, and thus the ribosome fraction can be expressed as

$$E_{\alpha,i} = \frac{m\nu_{\alpha,i}\phi_{P,i}}{n_P} = \frac{m\nu_{\alpha,i}(1 - \phi_{R,i} - \phi_Q)}{n_P}, \tag{9}$$

where $\nu_{\alpha,i}$ is species i's proportional expression of reaction α and satisfies $\sum_{\alpha \in O_i} \nu_{\alpha,i} = 1$, $\phi_{P,i}$ is species i's metabolic protein fraction, and n_P is the mass (average number of amino acids) of a metabolic protein [10]. The reaction rate in Eq 8 is derived by assuming a reversible kinetic scheme (full derivation in S1 Appendix) and can be expressed as

$$q_{\alpha,i}(E_{\alpha,i}, S_\alpha, W_\alpha) = \frac{k_{\alpha,i} E_{\alpha,i} S_\alpha (1 - \theta_i(S_\alpha, W_\alpha))}{K_{S_\alpha,i} + S_\alpha(1 + r_{\alpha,i}\theta_i(S_\alpha, W_\alpha))}, \tag{10}$$

where $k_{\alpha,i}$ is the maximum forward rate for reaction α for species i, $K_{S_\alpha,i}$ is species i's substrate half saturation constant for reaction α, $r_{\alpha,i}$ is species i's reversibility factor for reaction α, and $\theta_i(S_\alpha, W_\alpha)$ is a thermodynamic factor. This factor quantifies how far from equilibrium the reaction is, taking a value of 1 at equilibrium and tending towards 0 far from equilibrium. This thermodynamic factor is given by

$$\theta_i(S_\alpha, W_\alpha) = \frac{Q(S_\alpha, W_\alpha)}{\mathcal{K}_{\alpha,i}}, \tag{11}$$

where $Q(S_\alpha, W_\alpha)$ is the reaction quotient, which in the single reactant single product case we consider, is defined as $Q(S_\alpha, W_\alpha) = W_\alpha / S_\alpha$, and $\mathcal{K}_{\alpha,i}$ is species i's equilibrium constant for reaction α. Finally, we wish to consider the impact the species have on the environmental metabolite concentrations through the production and consumption of metabolites (process 2 in Fig 1A). From the expression for reaction rate the consumption and production rates for metabolite β that appear in Eq 1 can be defined as

$$p_{i,\beta}(\mathbf{C}) = \sum_{\alpha \in O_i} \delta_{C_\beta, W_\alpha} q_{\alpha,i}(E_{\alpha,i}, S_\alpha, W_\alpha), \tag{12}$$

and

$$c_{i,\beta}(\mathbf{C}) = \sum_{\alpha \in O_i} \delta_{C_\beta, S_\alpha} q_{\alpha,i}(E_{\alpha,i}, S_\alpha, W_\alpha). \tag{13}$$

In the above $\delta_{C_\beta, W_\alpha}$ and $\delta_{C_\beta, S_\alpha}$ are Kronecker deltas that are zero unless metabolite β is the waste product of reaction α or metabolite β is the substrate of reaction α, respectively.

Free-energy dissipation and thermodynamic inhibition

Due to the thermodynamic reversibility of our model the amount of free energy dissipated effects reaction rates. It is therefore important to think carefully about the amount of energy that is obtained from a given reaction event, which is captured by the number of ATPs produced η. Cells can also transduce free energy by pumping ions across membranes. Hence, we assume the minimum value this parameter can take is $\eta = 1/3$, which is approximately equivalent to the amount of free energy transduced by pumping one ion across a membrane. The maximum possible η value corresponds to all of the free energy being transduced to ATP and none of it being dissipated. However, in this case the overall reaction will be at equilibrium and there will be no net production of ATP. This impact of free energy dissipation on the dynamics occurs through the equilibrium constant which is specified as

$$\mathcal{K}_{\alpha,i} = \exp\left(\frac{-\Delta_\alpha G^0 - \eta_{\alpha,i}\Delta G_{\mathrm{ATP}}}{RT}\right), \tag{14}$$

where T is the temperature, R is the gas constant, ΔG_{ATP} is the Gibbs free energy per mole of ATP, and $\Delta_\alpha G^0$ is the standard Gibbs free energy change when one mole of reaction α occurs. As η changes the reaction rate (Eq 10) changes due to the change in this equilibrium constant. An example of the impact this has on the ATP production rate is visualised in Fig 1C. For low η values the equilibrium constant is very large so there is a negligible thermodynamic impact on the dynamics, and thus ATP production rate initially scales linearly with η. However, the exponential form of the equilibrium constant means that there is only a narrow region with anything other than negligible or complete thermodynamic inhibition. This means that ATP production peaks and then rapidly declines to zero as η increases. Though the narrowness of this peak leaves little room for alternative thermodynamic strategies, its position is determined by the waste product concentration allowing new types of interactions between species.

We make a number of observations. Firstly, from Fig 1C the naive conclusion that thermodynamic inhibition is unlikely to matter because it only occurs for a narrow range of η values could be drawn. However, all living things are under significant selection to maximise their energetic intake, this would like push real world microbial strains towards the limit where thermodynamic inhibition starts to matter. Secondly, when the free energy dissipated by the reaction is high the equilibrium constant (Eq 14) becomes very large meaning that thermodynamic inhibition plays no significant role. So when η is low relative to the Gibbs free energy change the kinetic scheme is effectively Michaelis–Menten, which explains why this scheme is appropriate to model many (but not all) ecosystems. Finally, the Gibbs free energy change between metabolites in the hierarchy is a key parameter. Microbes growing upon labile substrates (high free-energy availability) will both have faster growth and be less effected by thermodynamic inhibition compared to those growing on recalcitrant substrates (low free-energy availability).

The possible types of interaction and the mechanisms that lead to them are visualised in Fig 1D. Similarly to other microbial consumer-resource models [14–16] species in our model can interact by competing for the same substrate (competition) or by one species producing a metabolite that the other uses as a substrate (facilitation). However, due to the possibility of thermodynamic inhibition interactions via waste products (rather than substrates) are now possible. Strains can additionally interact by one species producing a product that thermodynamically inhibits the other species (pollution), or by one species consuming a product that inhibits the other (syntrophy). These interactions are determined by perturbing each metabolite in turn at steady state, and finding the response of each species. Then the net impact of each species on the concentration of each metabolite is found, which can be combined with the perturbation

response to find interactions strength between each species for each metabolite. The interaction types are then classified using the sign of the perturbation response and the whether the species makes a net positive or negative impact on the concentration of the perturbed metabolite (for a the full process see S1 Appendix).

It is finally worth noting that explicitly considering thermodynamic reversibility in our model allows the entropy production rate (free-energy dissipation rate) to be directly calculated. This is done by first calculating the free energy dissipation for species i per reaction event of reaction α by

$$D_{i,\alpha} = \Delta_\alpha G^0 + RT \ln\left(Q(S_\alpha, W_\alpha)\right) + \eta_{\alpha,i} \Delta G_{\mathrm{ATP}}, \tag{15}$$

and the whole ecosystem entropy production rate then becomes

$$\frac{dG_d}{dt} = \sum_{i=1}^{B} \left(\sum_{\alpha \in O_i} \left[\frac{D_{i,\alpha} q_{\alpha,i}(E_{\alpha,i}, S_\alpha, W_\alpha)}{T} \right] N_i \right). \tag{16}$$

This expression allows us to calculate the rate that the entire ecosystem is producing entropy. Without the overall summation the entropy production of individual species can also be found. The overall entropy production can potentially be used as a state variable to simplify the complex ecosystem dynamics in a physically meaningful manner.

Simulation procedure

To simulate the process of ecosystem assembly we numerically integrated a large system of ordinary differential equations (ODEs). This system consists of an ODE describing each of the M metabolites (Eq 1), and then for each of the B strains an ODE describing the dynamics of the population (Eq 4), the ribosome fraction (Eq 5) and the internal energy (Eq 7) was included, resulting in a system of $M + 3B$ equations. We generated the (M metabolite) reaction networks used in these simulations by following the pattern shown in Fig 1B, with the free-energy spacing of each step downwards in the metabolite hierarchy being equal. For each ecosystem we then generated a random community of B species. This was done by assigning each strain a number of reactions (N_O) drawn randomly from a uniform distribution. We then generated a reaction set (O) for each species by drawing N_O reactions at random from the full reaction network. We assigned random kinetic parameters (k, K_S and r) to each reaction for each species, drawn from normal distributions. Subsequently, we set the relative reaction expressions (ν) by assigning each reaction a uniformly distributed random number, which we then normalised by the sum of these across all reactions for the species in question. The next step was to assign the η values to each reaction that the species possesses. For this purpose, we randomly chose these from a uniform range between the minimum value ($\eta = 1/3$) and a maximum value which varies based on whether we were considering Michaelis–Menten or reversible kinetics. If we considered Michaelis–Menten kinetics, then the maximum possible value of η was chosen such that the reaction will reach equilibrium at a product to substrate ratio of 1×10^5. If instead we considered reversible kinetics, the maximum possible value of η was chosen such that the reaction will reach equilibrium at a product to substrate ratio of 1×10^{-2}. After we had generated the random communities, we began the simulation with every species having an equal population and ran them to a sufficiently late time (1×10^8 seconds) to ensure that the dynamics reached steady state. This procedure was repeated to generate replicate ecosystems.

Results

To demonstrate the dynamical behaviour of our model we show early dynamics of a particular parameter set in Fig 2. This specific simulation is started with an initial community of 250 species, each of which is assigned between 1 and 5 reactions from a 25 metabolite (47 reaction) network. The communities are generated with a reversible kinetic scheme, and the total free energy change from highest to lowest metabolite is $5.0 \times 10^6\,\mathrm{J\,mol^{-1}}$.

Fig 2A shows the population dynamics of the species that survive to steady state, and additionally the dynamics of a small number of species that go extinct. As the form of growth in Eq 4 is exponential all growth and decay curves are exponential, with exponents that shift as metabolites become more or less available. The dynamics of the ribosome fractions (Eq 5) corresponding to these species are shown in Fig 2B. When metabolite conditions are favourable to a species its internal energy concentration increases. According to Eq 6 this leads to an increase in the ribosome fraction and hence a higher growth rate. All species that survive to steady state settle down to an approximately equal ribosome fraction which is sufficient to balance the biomass loss term. In Fig 2C the metabolite concentration dynamics (Eq 1) for this ecosystem are shown. Initially, the single supplied metabolite accumulates, but as the population of species using this metabolite increase its concentration decreases and the concentration of metabolites one or two steps down the hierarchy increase. This process repeats leading to a sequential diversification of substrates, which leads to clear shifts in the ribosome fraction and population dynamics. One of these shifts is indicated by the red line shown in all panels, which marks the point where metabolite 3 is first above the threshold to support growth. To show the generality of this diversification, the initial and final distributions of the number of utilisable substrates (across 250 simulations) are shown as an inset to Fig 2C. In Fig 2D the rate of ecosystem entropy production (Eq 16) is plotted. The entropy production rises as the substrate diversifies and the total population increases, and shows clear peaks at the time points where accumulated substrates are rapidly depleted. It can be considered a low-dimensional summary read out or characteristic signature of an evolving ecosystem.

Final ecosystem states dependant on free-energy availability

The large number of initial species makes visualisation of the diversity loss with time difficult. So in order to better visualise diversity loss with time we now group species into coarse functional groups, based on the substrate used by their most expressed reaction. The relative abundance of these functional groups with time is shown for an example parameter set in Fig 3A (with the same simulation parameters as Fig 2). The functional diversity initially collapses and then slowly relaxes towards steady state. This mirrors the time series obtained over successive dilution events shown by Goldford et al. [15]. To quantify the diversity across simulation runs we consider the inverse Simpson diversity index, which corresponds to the effective number of types (here functional groups) in an ecosystem. The inset histogram of initial and final distribution of this index shows that functional diversity collapse is common across our simulations.

The final ecosystem states are now compared across four different conditions in Fig 3B. The conditions compared are low and high substrate free energy, and whether the enzyme kinetics are Michaelis–Menten or reversible. This is done for a number of final ecosystem properties, which are each averaged over 250 simulation runs with 99% confidence interval shown. All species in these simulations have between 1 and 5 reactions, and each simulation is started with 250 species. The first property compared is the number of surviving functional groups. Systems supplied with a substrate of higher free energy see a greater number of surviving functional groups. Using a

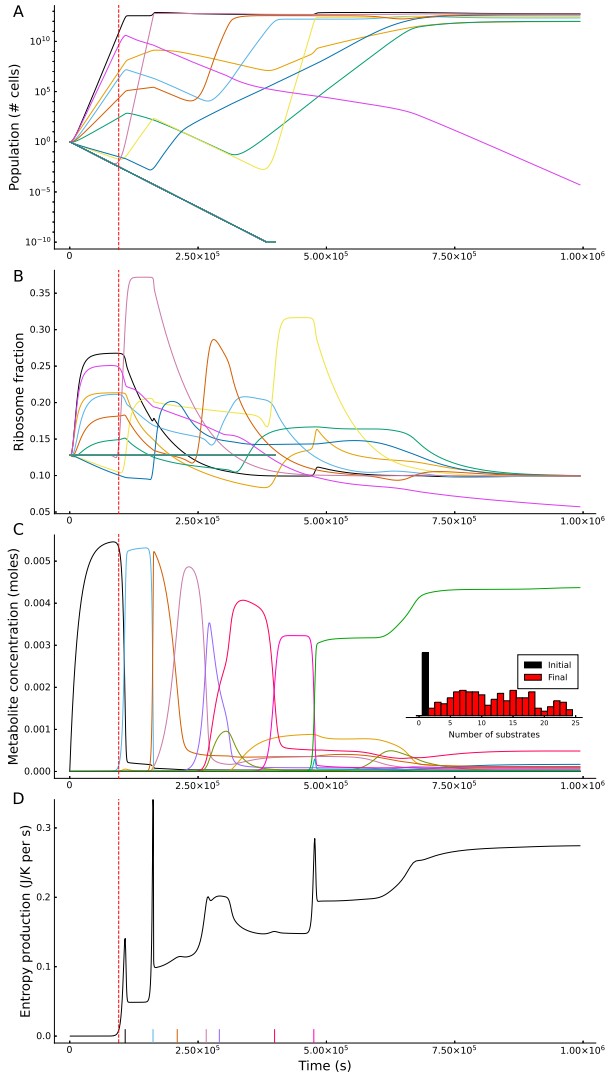

Fig 2. Key dynamical signature of model. (a) Populations vs time. The dynamics of all surviving species are shown, alongside the dynamics of a few of the many species that are driven to extinction. (b) Corresponding graph of ribosome fraction with time. All species that survive to steady state settle to the same ribosome fraction in order to balance the fixed biomass loss rate. (c) Corresponding metabolite dynamics, in contrast to the population dynamics this is shown on a linear scale for the sake of clarity. Thus, the changes appear much more rapid on this graph compared to the population graph. The inset shows distributions of the initial and final number of metabolites across 250 simulations. (d) Entropy production rate of the ecosystem with time. The marks on the x-axis correspond to time points where accumulated metabolites drop below an exhaustion threshold (2×10^{-3} moles). The color coding corresponds to the metabolite plot. The red lines shown across all plots correspond to the time point where the third metabolite is available in sufficient quantity (1×10^{-4} moles) to support growth. The parameter set used here was one of the 250 parameter sets generated using a reversible kinetic scheme and a total free energy change of $5.0 \times 10^{6}\,\mathrm{J\,mol^{-1}}$.

reversible kinetic scheme (rather than Michaelis–Menten) only increases the number of surviving functional groups in the low free-energy case. A nearly identical pattern is

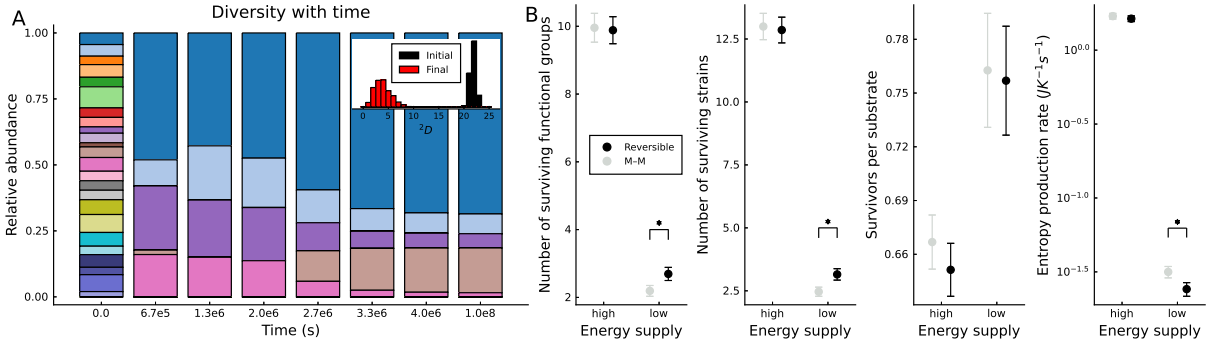

Fig 3. Impact of free-energy on the diversity. (a) Plot of relative abundances of species grouped by preferred substrate (a proxy for functional group) over time. The inset show initial and final distributions of inverse Simpson's diversity indices for functional groups across 250 simulations (using the same simulation parameters as Fig 2). (b) A series of plots making comparisons between four conditions. For each condition the average and 99% confidence interval obtained from 250 simulations are plotted. The first plot compares number of surviving functional groups between conditions. The second plot compares the number of surviving species between conditions. In the third plot the number of surviving species per final number of substrates diversified is compared across conditions. In the fourth plot for all the conditions entropy production is compared. Two different values of the total free energy of the supplied substrate are considered: high ($1.5 \times 10^7\,\mathrm{J\,mol^{-1}}$), and low ($1.5 \times 10^6\,\mathrm{J\,mol^{-1}}$). For both energy conditions we consider both reversible (black symbols) and Michaelis–Menten (M–M grey symbols) kinetics. Cases where there is a significant difference between these pairs are marked with a star ($P < 0.01$).

observed for the number of surviving species, suggesting that the decline in functional diversity is predominantly driven by a decline in species diversity. To test whether high energy substrates can support more species we then compared the ratio between the number of surviving species and the number of substrates diversified to. We found that the number of survivors per substrate is lower for high free energy substrates, with no significant difference between kinetic schemes. For the ecosystem entropy production rate, higher substrate free energy corresponds to higher entropy production rates. There is again only a significant difference between kinetic schemes when substrate free-energy is low. These results suggest that only in this case do the two schemes result in ecosystems with meaningfully different thermodynamic properties.

Free-energy availability increases rate of ecosystem succession

The naive explanation for the diversity results in Fig 3B is that higher free energy availability increases the chance of a species being viable on a particular substrate. However, this is clearly contradicted by the surviving species per substrate results shown in Fig 3B. A more careful investigation of the mechanism that sustains diversity is displayed in Fig 4. In order to better display this mechanism only a small initial time window of the dynamics is shown. For each of the four conditions considered in Fig 3 averages and 99% confidence intervals of variables are plotted against time (across 250 simulations). The first variable we consider is the number of surviving species, which is shown in Fig 4A. All conditions show a significant loss in species diversity at a specific time. This is the time point where species that never grow at all reach extinction. The number of surviving species drops to a significantly lower value across all conditions and then levels out, remaining at a substantially higher level at high substrate free energy. At low substrate free energy a small but significant difference in the number of survivors between the reversible and Michaelis–Menten conditions can be seen to emerge after the mass extinction event.

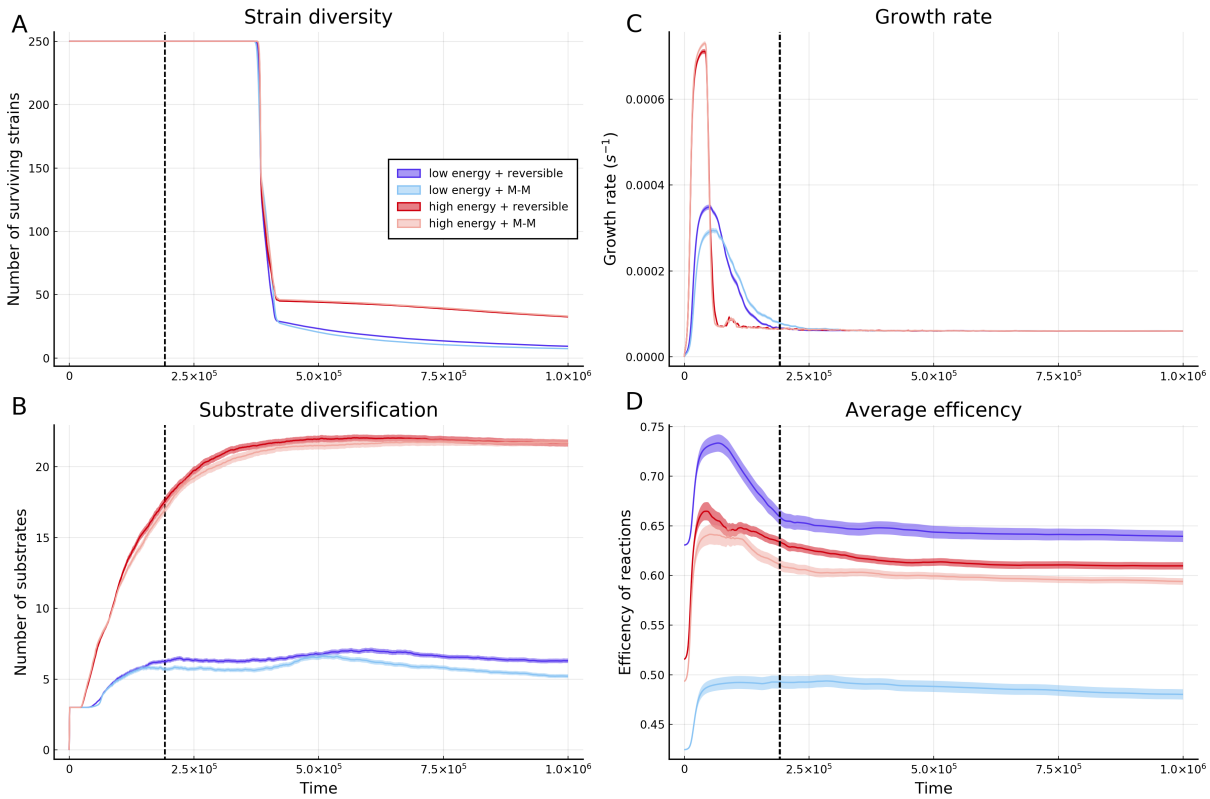

Fig 4. Average developmental time course of the ecosystems. (a) Graph showing average species diversity over time for the four conditions from Fig 3 (with 99% confidence intervals). The dashed black line (shown in all four plots) indicates the time point where 75% of species have dropped below the viability threshold. (b) Average substrate diversification over time. (c) Average growth rate over time. (d) Average reaction efficiency over time. The timings of the peaks here can be seen to match with the growth rate peaks. The four plots use the same parameters for the respective conditions as are used in Fig 3.

To understand these dynamics we now consider the substrate diversification with time, shown in Fig 4B. For all conditions the number of substrates can be seen to rapidly plateau. The black line shows the time point where 75% of species have dropped below the threshold to be considered viable. The plateau occurs after the point where the majority of species can no longer contribute to the substrate dynamics. At high substrate free energy the plateau occurs at a far higher number of substrates than at low substrate free energy, and at low substrate free energy the reversible case plateaus slightly higher than the corresponding Michaelis–Menten case. This mirrors the species diversity shown in Fig 4A, suggesting that diversity is driven by the number of available substrates. The average growth rates for the four conditions are shown in Fig 4C. All conditions show an initial period of rapid growth while the energy availability per species is high which settles down to a steady growth rate as the total population increases. The most pronounced peaks are seen at high substrate free energy due to the greatly increased energy availability. There is a small difference in peak height at low substrate free energy as allowing reactions close to equilibrium leads to greater free energy extraction from the environment. These differing growth rate account for the differing rates of substrate diversification seen in Fig 4B.

The strategy of allowing near-equilibrium reactions increases free energy yield, but carries the risk of reactions becoming thermodynamically unfeasible. To ascertain the

importance of this effect we plot average reaction efficiencies with time in Fig 4D. The average thermodynamic efficiency of the community can change through a process of species sorting, as the proportional abundance of species with differing average reaction efficiencies changes. Species sorting drives an increase in average reaction efficiency during the initial growth period across all conditions, as strains with highly efficiency reactions yield more free energy, and thus grow faster. The two low free energy cases are substantially further apart than the two high free energy cases. This arises because low free energy reactions are inherently closer to equilibrium. Hence, the reversible case has higher efficiency because its closer to equilibrium, and the efficiency of the Michaelis–Menten case is reduced more significantly to ensure reactions are far from equilibrium. In the reversible low free energy case, after the initial period waste products accumulate and reactions become thermodynamically inhibited, a sharp efficiency peak is created. In the corresponding Michaelis–Menten case the reactions are always far-from-equilibrium and so this inhibition never occurs and the efficiency simply plateaus. As the higher free energy cases are generally further from equilibrium, the pattern here is likely driven by a transition from an initial highly efficient community that breaks down the initial substrate to more diverse community that breaks down a wider range of secondary substrates. This community is less thermodynamically efficient as the broader range of substrate means that energetic competition is weaker.

Thermodynamic interaction types impact dynamics

To confirm that thermodynamics plays a significant role in the dynamics we determined the relative prevalence and strengths of the different interaction types from Fig 1D. The method of determining interaction types and determining their strengths is set out in S1 Appendix. The proportion and strength of interactions are shown for an intermediate substrate free energy ($1.5 \times 10^6\,\mathrm{J\,mol^{-1}}$) in Fig 5. In Fig 5A the relative proportions of competition, facilitation, and thermodynamic (pollution and syntrophy) interactions are plotted on a simplex. This is for a case with Michaelis–Menten kinetics and it can be seen that competition interactions are the most common, and that thermodynamic and facilitation interactions tend occur with similar frequency. In Fig 5B histograms of the interaction strengths are shown for each interaction type. There is a clear separation of scales between the two non-thermodynamic (competition and facilitation) interaction types and the two thermodynamic ones (syntrophy and pollution). This can be seen clearly by the position of the red line which marks the distribution's right-hand half-maximum, which is several orders of magnitude below the peak of the competition and facilitation distributions. Fig 5C also shows the relative proportions of the different interaction types but this time for reversible kinetics. Competition interactions remain the most common, but now thermodynamic interactions are now marginally more common than facilitation interactions. The relative frequency of positive and competitive interactions is basically unchanged, but the proportion of thermodynamic interactions has increased. The difference is more pronounced in Fig 5D, which shows the interaction strengths for reversible kinetics. In this case the separation of scales between thermodynamic and non-thermodynamic interactions has disappeared implying a meaningful impact of thermodynamics on the dynamics. In S1 Fig the results are shown for the high free energy case, and the same overall pattern is seen. However, the proportion of thermodynamic interactions is significantly lower, as is the mean strength of the thermodynamic interactions relative to the non-thermodynamic interactions. This result matches our expectation from the fact that the kinetic scheme used had no significant effect on the ecosystem properties for high substrate free energy.

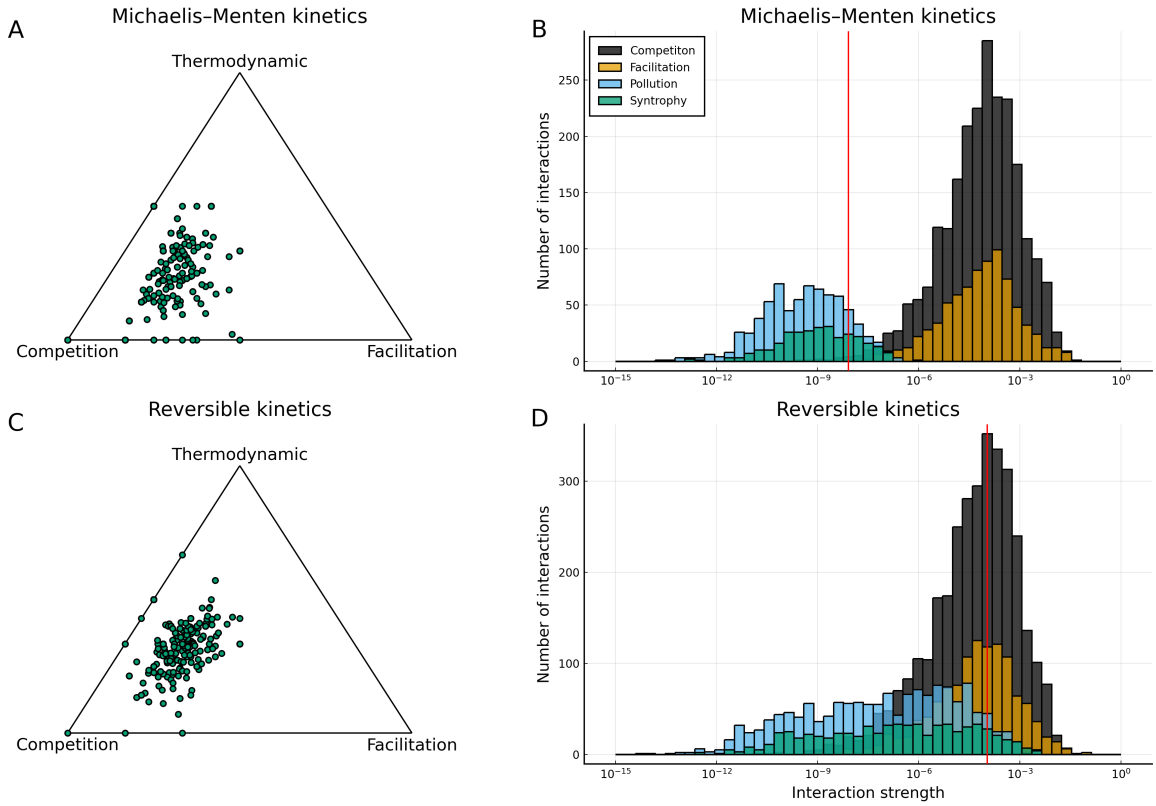

Fig 5. Thermodynamic and competitive interactions can be of comparable strength. (a) Simplex showing the relative proportions of competition, facilitation and the thermodynamic (pollution and syntrophy) interaction types, these interaction types are shown schematically in Fig 1D. Each point represents one out the 250 ecosystems we simulated for each condition. (b) Histogram of strengths of the four interaction types. The vertical red line marks the point where the distribution of the strengths of the pollution interaction is at half its maximum. (c) Corresponding plot to Fig 5A for reversible kinetics. (d) Corresponding plot to Fig 5B for reversible kinetics. All cases considered here are for the low free energy supply case ($1.5 \times 10^6\,\mathrm{J\,mol^{-1}}$).

Discussion

In this paper we investigated how the inclusion of thermodynamic reversibility effects the dynamics and final states of microbial ecosystems. We found (see Fig 2) population dynamics qualitatively similar to those seen in more traditional microbial consumer-resource models. Differences in final diversity were found to be driven primarily by the substrate free energy, and only in cases of low substrate free energy does allowing species to have near to equilibrium reactions effect the final diversity (see Fig 3). A mechanism explaining this effect was found in Fig 4, which was that high substrate free energy allowed for more rapid substrate diversification, meaning more niches can be created before species diversity collapses. We also find that when the free energy of the supplied substrate is low highly efficient species are selected for in the diversification stage, but after this stage they are disfavoured as they carry the risk of no longer being able to generate ATP due to their reactions reaching thermodynamic equilibrium. When comparing the types and strengths of interactions across ecosystems (Fig 5) we find that though thermodynamic interactions are rarer than non-thermodynamic interactions they can reach similar magnitudes. Thus, confirming

that thermodynamic interactions play a meaningfully role in the dynamics of at least some of the microbial ecosystems that we consider.

Substrates are often classified by the difficulty involved in breaking them down, with substrates easily broken down by microbes being termed labile and ones that are hard to break down termed recalcitrant. In energetic terms a recalcitrant substrate can thought of as one that requires a significant energy investment by the microbe for a minimal return. This could be a substrate with a high activation energy, or one that has to be broken down extracellularly, or as in our case a substrate that yields low free energy. Most microbes preferentially use labile substrates but shifts towards using recalcitrant substrates has been observed to occur both as temperature increases [17], and as ecosystems develop [18]. Our results suggest that the inclusion of thermodynamic reversibility only leads to significant differences in ecosystem properties (see Fig 3B) for recalcitrant (low free energy) substrates. This arises because when free energy is readily available the advantage of taking a high efficiency strategy is much lower, while this strategy still carries the risk of reactions becoming thermodynamically unfeasible. Thus, species using highly efficient reactions are competitively disadvantaged and therefore do not have a significant impact on the dynamics.

In addition to this we would expect thermodynamic effects to be far more important for anaerobic than aerobic ecosystems, due to the lower free energy availability, which is consistent with the fact that previous models incorporating thermodynamic inhibition have been for anaerobic systems [4, 5]. However, the frequent usage of recalcitrant substrates by microbes means our model is relevant beyond anaerobic systems. For labile substrates frequently used in lab cultures a non-thermodynamic model would be entirely appropriate, but when modelling growth on recalcitrant substrates thermodynamic effects are likely to be important. We suspect that understanding thermodynamic effects will be a necessary step towards understanding microbial succession dynamics. Particularly in cases where the predominately available substrate type changes as the succession progresses [19, 20].

In this modelling framework we aimed to avoid the common limitation of microbial populations either being treated as having no internal dynamics or being assigned complete (and extremely complex) internal dynamics [21]. Our model introduced an intermediate level of complexity by drawing on the widely known effect of proteome trade-offs on growth [8–10]. More detailed investigation of the effect of this constraint on the dynamics and how it links to related trade-offs such as 16S copy number is a promising avenue for future work. Beyond this there are many other cellular constraints and trade-offs that could be fruitfully incorporated as intermediate dynamics for microbial consumer-resource models.

Our model fits into a growing body of models that are extensions of MacArthur's consumer-resource model [13]. In contrast to our approach some of these models do not include metabolite production and cross-feeding at all [22]. In some approaches cross feeding and metabolite production is considered but growth is dependant on obtaining specific metabolites rather than free energy [16]. Approaches that consider energy are also common, though some of these introduce tight constraints on the number of metabolites a strain can consume [23]. Most similar to our model are approaches where strains are assumed to consume a wide variety of metabolites, which both yields energy for the microbes and produces secondary metabolites [14, 15]. Our approach differs from this mainly through the inclusion of stricter thermodynamic constraints and more realistic proteome constraints.

There has been much historic discussion in literature of the so called "paradox of the plankton" [24]. This paradox refers to the apparent contradiction between the expectation from competitive exclusion theory of one surviving species per limiting resources, and the huge diversity of plankton observed. Many potential resolutions to

this paradox have been proposed such as chaotic dynamics [25], temporal heterogeneity [26], spatial heterogeneity [27], limitation by factors other than resource availability (e.g. predation) [28], or rapid evolution [29]. Recent work has suggested that both thermodynamic inhibition [6] and metabolic trade-offs [7] can allow more survivors than substrates, though it has since been suggested that metabolic trade-offs only support increased diversity for a very narrow and specific parameter range [30]. The proteomic trade-off that our model includes represents a more detailed version of the metabolic trade-off previous work has considered, where instead of a fixed "enzyme budget" the fraction of the proteome that is available to split between reactions inversely proportional to the size of the ribosome fraction. Due to our model also including thermodynamic inhibition, it represents a natural means to test if these increased diversities are retained in larger and more realistic stochastically generated ecosystems. From Fig 3B it can be seen that the average number of survivors is always lower than the average number of available substrates. Across the 1000 simulations we performed in no case does the number of survivors exceeded the number of diversified substrates (see S2 Fig), suggesting that competitive exclusion is not violated. Our results suggest that though metabolic or thermodynamic trade-offs can offer a solution to "the paradox of the plankton" in special cases this is not a general effect. This paradox is far more likely to be resolved by the spatial and temporal heterogeneity of real ecosystems.

Conclusion

By developing a thermodynamic microbial consumer-resource model we investigated the constraints that non-equilibrium thermodynamics places upon ecosystems. We found that the speed of ecosystem development was strongly coupled to the availability of free energy. Faster development allows for greater diversity as new niches arise more quickly, increasing the chance a species can successfully establish itself. We also found that only for low free energy substrates did allowing near-to-equilibrium reactions significantly increase the availability of free energy, and thus the diversity. However, these reactions exist at far greater risk of thermodynamic inhibition and so after the initial phase of ecosystem establishment they are disfavoured. Finally, we discovered that under certain conditions thermodynamic interactions could reach similar strengths to conventional interactions, underlining the fact that thermodynamic effects play a meaningful role in the overall ecosystem dynamics. Taken together our results indicate that thermodynamic inhibition does act to constrain the diversity of ecosystems when free energy is scarce.

Supporting information

S1 Appendix. Supplementary text. This supporting text contains a comparison of Michaelis–Menten and reversible enzyme kinetic schemes, a full derivation of the proteome trade-off model and the method used for identifying interactions and quantifying their strengths.

S1 Fig. Interactions high energy case. Identical plot to Fig 5 but for the high energy supply case ($1.5 \times 10^7\,\mathrm{J\,mol^{-1}}$).

S2 Fig. Test of competitive exclusion. Plot of the number of surviving species against the total number of substrates diversified by the time steady state is reached. This shows the full data from across all four conditions considered in the main text, e.g.

1000 simulation runs in total. In no case does the number of survivors exceed the number of substrates (equality indicated by the red line).

Acknowledgments

Here we thank Tom Clegg, Alexander Christensen, Paul Huxley, Pablo Lechón, and Thomas P. Smith for helpful discussions and comments on the draft manuscript, and financial support from the NERC CDT in Quantitative and Modelling Skills in Ecology and Evolution (grant No./ NE/P012345/1).

References

1. Piñeros WD, Tlusty T. Kinetic proofreading and the limits of thermodynamic uncertainty. Phys. Rev. E. 2002 Feb;101(2): 022415. doi: 10.1103/PhysRevE.101.022415.

2. Tu, Y. The nonequilibrium mechanism for ultrasensitivity in a biological switch: Sensing by Maxwell's demons. PNAS. 2008 Aug;105(33): 11737–11741. doi: 10.1073/pnas.0804641105.

3. Phillips SJ, Anderson RP, Schapire RE. Maximum entropy modeling of species geographic distributions. Ecol. Model. 2006 Jan;190(3-4): 231–259. doi: 10.1016/j.ecolmodel.2005.03.026.

4. Hoh CY, Cord-Ruwisch R. A practical kinetic model that considers endproduct inhibition in anaerobic digestion processes by including the equilibrium constant. Biotechnol. Bioeng. 1996 Sep;51(5): 597–604. doi: 10.1002/(SICI)1097-0290(19960905)51:5<597::AID-BIT12>3.0.CO;2-F.

5. Lynch TA, Wang Y, van Brunt B, Pacheco D, Janssen PH. Modelling thermodynamic feedback on the metabolism of hydrogenotrophic methanogens. J. Theor. Biol. 2019 Sep;477:14–23. doi: 10.1016/j.jtbi.2019.05.018.

6. Großkopf T, Soyer OS. Microbial diversity arising from thermodynamic constraints. ISME J. 2016 Nov;10(11): 2725–2733. doi: 10.1038/ismej.2016.49.

7. Posfai A, Taillefumier Thibaud, Wingreen NS. Metabolic trade-offs promote diversity in a model ecosystem. Phys. Rev. Lett. 2017 Jan;118(2): 028103. doi: 10.1103/PhysRevLett.118.028103.

8. Scott M, Gunderson CW, Mateescu EM, Zhang Z, Hwa T. Interdependence of cell growth and gene expression: origins and consequences. Science. 2010 Nov;330(6007): 1099–1102. doi: 10.1126/science.1192588.

9. Scott M, Klumpp S, Mateescu EM, Hwa T. Emergence of robust growth laws from optimal regulation of ribosome synthesis. Mol. Syst. Biol. 2014 Aug;10(8): 747–747. doi: 10.15252/msb.20145379.

10. Weiße AY, Oyarzún DA, Danos V, Swain PS. Mechanistic links between cellular trade-offs, gene expression, and growth. PNAS. 2015 Mar;112(9): E1038–E1047. doi: 10.1073/pnas.1416533112.

11. Foster KR, Bell T. Competition, not cooperation, dominates interactions among culturable microbial species. Curr. Biol. 2012 Oct;22(19): 1845–1850. doi: 10.1016/j.cub.2012.08.005.

12. Machado D, Maistrenko OM, Andrejev S, Kim Y, Bork P, Patil KR, et al. Polarization of microbial communities between competitive and cooperative metabolism. Nat. Ecol. Evol. 2021 Feb;5(2):195–203. doi: 10.1038/s41559-020-01353-4.

13. MacArthur, R. Species packing and competitive equilibrium for many species. Theor. Popul. Biol. 1970 May;1(1): 1–11. doi: 10.1016/0040-5809(70)90039-0.

14. Marsland R, Cui W, Goldford J, Sanchez A, Korolev K, Mehta P. Available energy fluxes drive a transition in the diversity, stability, and functional structure of microbial communities. PLoS Comput. Biol. 2019 Feb;15(2): e1006793. doi: 10.1371/journal.pcbi.1006793.

15. Goldford JE, Nanxi L, Djordje B, Estrela S, Tikhonov M, Sanchez-Gorostiaga A, et al. Emergent simplicity in microbial community assembly. Science. 2018 Aug;361(6401): 469–474. doi: 10.1126/science.aat1168.

16. Taillefumier T, Posfai A, Meir Y, Wingreen NS. Microbial consortia at steady supply. eLife. 2017 May;6: e22644. doi: 10.7554/eLife.22644.

17. Frey SD, Lee J, Melillo JM, Six J. The temperature response of soil microbial efficiency and its feedback to climate. Nat. Clim. Change. 2013 Apr;3(4): 395–398. doi: 10.1038/nclimate1796.

18. Rivett DW, Scheuerl T, Culbert CT, Mombrikotb SB, Johnstone E, Barraclough TG, et al. Resource-dependent attenuation of species interactions during bacterial succession. ISME J. 2016 Sep;10(9): 2259–2268. doi: 10.1038/ismej.2016.11.

19. Datta MS, Sliwerska E, Gore J, Polz MF, Cordero OX. Microbial interactions lead to rapid micro-scale successions on model marine particles. Nat. Commun. 2016 Jun;7(1): 11965. doi: 10.1038/ncomms11965.

20. Enke TN, Datta MS, Schwartzman J, Cermak N, Schmitz D, Barrere J, et al. Modular assembly of polysaccharide-degrading marine microbial communities. Curr. Biol. May 2019;29(9):1528–1535.e6. doi: 10.1016/j.cub.2019.03.047.

21. Liao C, Wang T, Maslov S, Xavier JB. Modeling microbial cross-feeding at intermediate scale portrays community dynamics and species coexistence. PLoS Comput. Biol. 2020 Aug;16(8): e1008135. doi: 10.1371/journal.pcbi.1008135.

22. Tikhonov M. Community-level cohesion without cooperation. eLife. 2016 Jun;5: e15747. doi: 10.7554/eLife.15747.

23. Goyal A, Maslov S. Diversity, stability, and reproducibility in stochastically assembled microbial ecosystems. Phys. Rev. Lett. 2018 Apr;120(15): 158102. doi: 10.1103/PhysRevLett.120.158102.

24. Hutchinson GE. The paradox of the plankton. Am. Nat. 1961 May;95(882): 137–145. doi: 10.1086/282171.

25. Huisman J, Weissing FJ. Biodiversity of plankton by species oscillations and chaos. Nature. 1999 Nov;402(6760): 407–410. doi: 10.1038/46540.

26. Descamps-Julien B, Gonzalez A. Stable coexistence in a fluctuating environment: an experimental demonstration. Ecology. 2005 Oct;86(10): 2815–2824. doi: 10.1890/04-1700.

27. Huisman J, van Oostveen P, Weissing FJ. Species dynamics in phytoplankton blooms: incomplete mixing and competition for light. Am. Nat. 1999 Jul;154(1): 46–68. doi: 10.1086/303220.

28. Roughgarden J, Feldman M. Species packing and predation pressure. Ecology. 1975 Mar;56(2): 489–492. doi: 10.2307/1934982.

29. Yamamichi M, Letten AD. Rapid evolution promotes fluctuation-dependent species coexistence. Ecol. Lett. 2021 Apr;24(4): 812–818. doi: 10.1111/ele.13707.

30. Li Z, Liu B, Li SH-J, King CG, Gitai Z, Wingreen NS. Modeling microbial metabolic trade-offs in a chemostat. PLoS Comput. Biol. 2020 Aug;16(8): e1008156. doi: 10.1371/journal.pcbi.1008156.